CM² MAGAZINE

第 116 期

南方科技大学海洋磁学中心主编

http://cm2.sustech.edu.cn/

创刊词

海洋是生命的摇篮，是文明的纽带。地球上最早的生命诞生于海洋，海洋里的生命最终进化成了人类，人类的文化融合又通过海洋得以实现。人因海而兴。

人类对海洋的探索从未停止。从远古时代美丽的神话传说，到麦哲伦的全球航行，再到现代对大洋的科学钻探计划，海洋逐渐从人类敬畏崇拜幻想的精神寄托演变成可以开发利用与科学研究的客观存在。其中，上个世纪与太空探索同步发展的大洋科学钻探计划将人类对海洋的认知推向了崭新的纬度：深海（deep sea）与深时（deep time）。大洋钻探计划让人类知道，奔流不息的大海之下，埋藏的却是亿万年的地球历史。它们记录了地球板块的运动，从而使板块构造学说得到证实；它们记录了地球环境的演变，从而让古海洋学方兴未艾。

在探索海洋的悠久历史中，从大航海时代的导航，到大洋钻探计划中不可或缺的磁性地层学，磁学发挥了不可替代的作用。这不是偶然，因为从微观到宏观，磁性是最基本的物理属性之一，可以说，万物皆有磁性。基于课题组的学科背景和对海洋的理解，我们对海洋的探索以磁学为主要手段，海洋磁学中心因此而生。

海洋磁学中心，简称 CM^2，一为其全名“Centre for Marine Magnetism”的缩写，另者恰与爱因斯坦著名的质能方程 $E = MC^2$ 对称，借以表达我们对科学巨匠的敬仰和对科学的不懈追求。

然而科学从来不是单打独斗的产物。我们以磁学为研究海洋的主攻利器，但绝不仅限于磁学。凡与磁学相关的领域均是我们关注的重点。为了跟踪反映国内外地球科学特别是与磁学有关的地球科学领域的最新研究进展，海洋磁学中心特地主办 CM^2 Magazine，以期与各位地球科学工作者相互交流学习、合作共进！

“海洋孕育了生命，联通了世界，促进了发展”。21 世纪是海洋科学的时代，由陆向海，让我们携手迈进中国海洋科学的黄金时代。

目录

1. 冰期-间冰期尺度上印度洋南部上层海洋水动力、生物地球化学和生产力变化

翻译人：仲义 zhongy@sustech.edu.cn

Tangunan, D., Berke, M. A., Cartagena-Sierra, A., et al. ***Strong glacial-interglacial variability in upper ocean hydrodynamics, biogeochemistry, and productivity in the southern Indian Ocean*** *[J] Nature Climate Change, 2021, 2(1), 80.*

https://doi.org/10.1038/s43247-021-00148-0

摘要：在印度洋南部地区，亚热带锋面的位置作为南部较冷、淡水和北部温暖、盐水的分界，对于上层海洋水动力和生物地球化学具有重要的影响。本文中，作者分析厄加勒斯高原上位于现代亚热带锋面带附近的沉积物钻孔，通过烯酮和颗石藻群落指标重建 30 万年来海洋环境变化。作者确定了海表温度和生产力变化冰期-间冰期的变化，且与阿古拉斯高原附近亚热带锋面移动密切相关，表现短期高频变化与高纬度日射量变化较为一致。结合硅藻和有机碳记录以及烯酮和颗石藻含量表现出冰期输出生产力升高的趋势。作者认为冰期生物泵作用增强，可能是大气 CO_2 浓度下降的部分原因。

ABSTRACT: In the southern Indian Ocean, the position of the subtropical front – the boundary between colder, fresher waters to the south and warmer, saltier waters to the north – has a strong influence on the upper ocean hydrodynamics and biogeochemistry. Here we analyse a sedimentary record from the Agulhas Plateau, located close to the modern position of the subtropical front and use alkenones and coccolith assemblages to reconstruct oceanographic conditions over the past 300,000 years. We identify a strong glacial-interglacial variability in sea surface temperature and productivity associated with subtropical front migration over the Agulhas Plateau, as well as shorter-term high frequency variability aligned with variations in high latitude insolation. Alkenone and coccolith abundances, in combination with diatom and organic carbon records indicate high glacial export productivity. We conclude that the biological pump was more efficient and strengthened during glacial periods, which could partly account for the reported reduction in atmospheric carbon

dioxide concentrations.

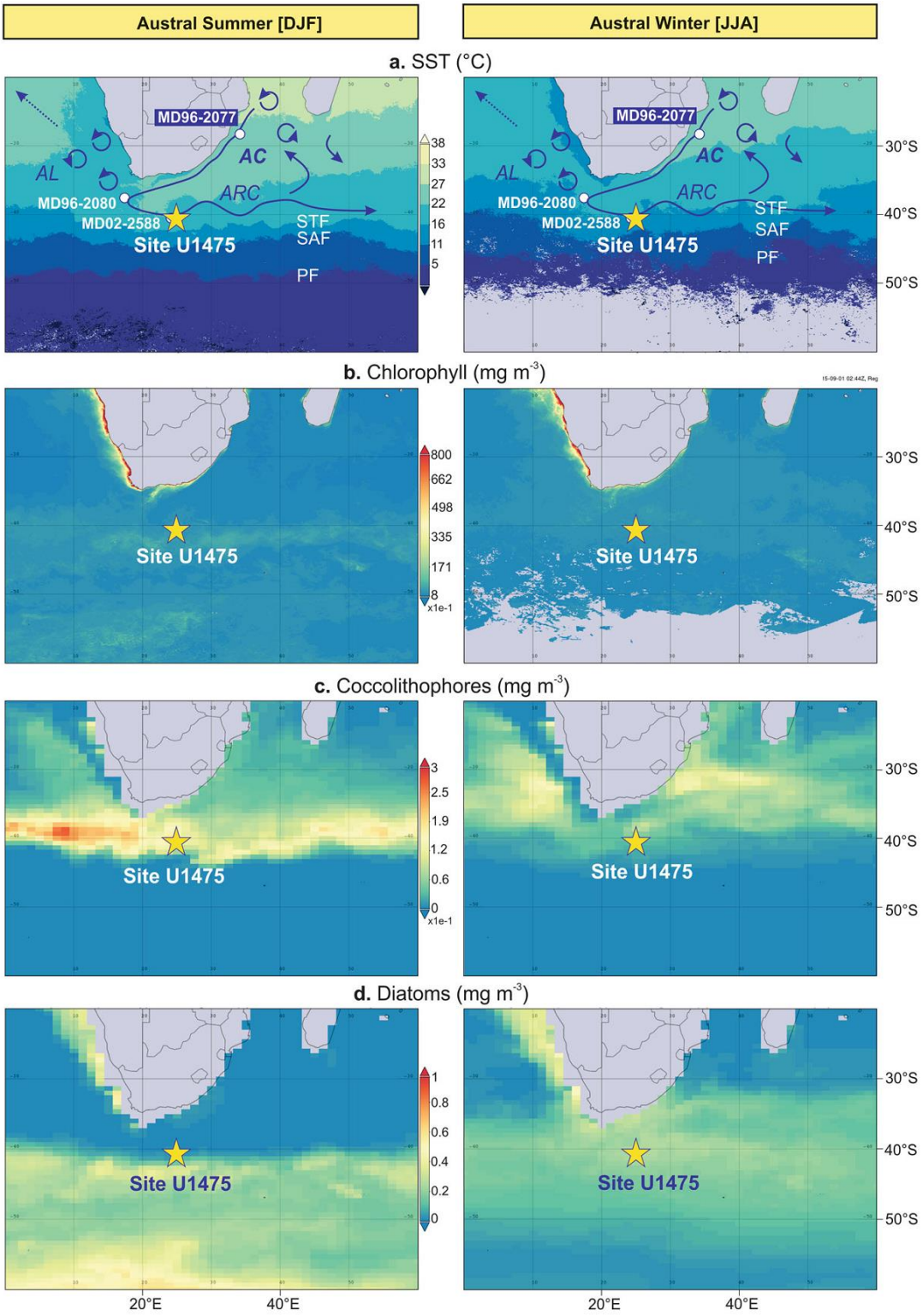

Figure 1. Modern-day oceanography at Site U1475 during austral summer (December-January-February, DJF) and austral winter (June-July-August, JJA) from 2013 to 2015. a Sea surface temperature (SST, °C) showing the study site (yellow star) and other core locations mentioned in

the text (white circles), together with the Southern Ocean and the southern Indian Ocean fronts: Subtropical Front (STF), Subantarctic Front (SAF) and Polar Front (PF), and the schematic representation of the average surface ocean circulation (Agulhas Current, AC; Agulhas Return Current, ARC; Agulhas Leakage, AL). b Chlorophyll-α concentrations (mg m^{-3}). c Coccolithophores (mg m^{-3}). d Diatoms (mg m^{-3}). Data, maps and visualisations were generated using the Giovanni online data system (https://giovanni.gsfc.nasa.gov/giovanni/) developed and maintained by the National Aeronautics and Space Administration Goddard Earth Sciences Data and Information Services Center (NASA GES DISC). The SST and chlorophyll data are derived from Moderate Resolution Imaging Spectroradiometer on the Aqua satellite (MODIS-Aqua) provided to Giovanni by the Ocean Biology Distributed Active Archive Center (OB. DAAC). The coccolithophore and diatom data are from the NASA Ocean Biogeochemical Model (NOBM).

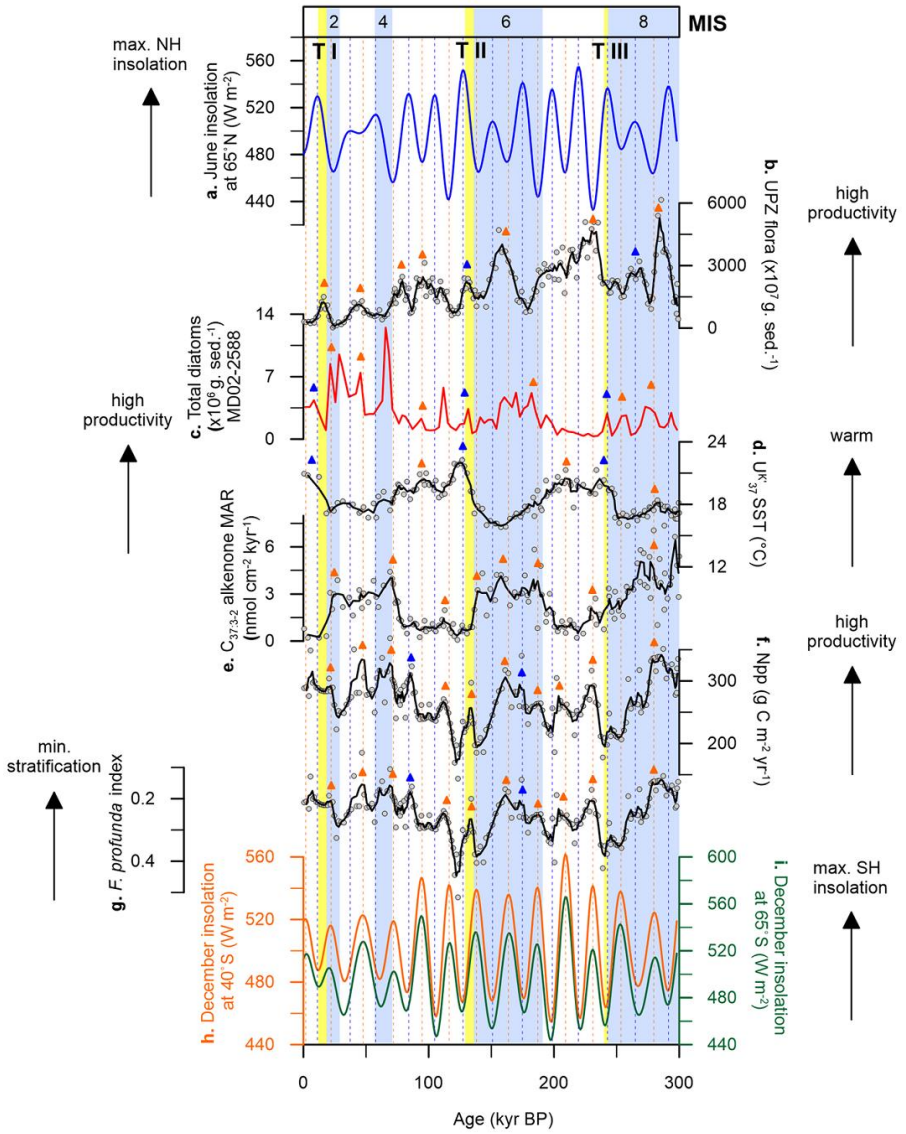

Figure 2. Paleoceanographic records at the Agulhas Plateau (Site U1475 and MD02-2588) plotted against regional and high latitude summer insolation. a Maximum summer insolation at the northern hemisphere (NH, 65°N, blue). b Upper photic zone (UPZ) flora (black). c MD02-2588 total diatoms (red). d U^{K}_{370} sea surface temperature (SST, black). e $C_{37:3\text{-}2}$ alkenone mass accumulation rate (MAR, black). f Net primary productivity (Npp, black). g Florisphaera profunda index (black). h Maximum summer insolation at Site U1475 (40°S, orange). i maximum summer insolation at the southern hemisphere (SH, 65°S, green). The coloured arrows represent coincidence between our records and summer insolation maxima in the NH (blue) and SH (orange). Solid lines are calculated five-point running average of the raw data (white circles) to highlight long-term trends. Light blue bars are glacial intervals (marine isotope stages, MIS). Yellow bars are glacial terminations (T).

2. 南海西北部始新世-中新世源汇系统的时空演化

翻译人：刘伟 inewway@163.com

Chao F, Shengli Li, Shunli Li, et al. ***Spatial-temporal evolution of the source-to-sink system in the northwestern South China Sea from the Eocene to the Miocene*** *[J]. Global and Planetary Change, 2022.*

https://doi.org/10.1016/j.gloplacha.2022.103851

摘要：南海西北部源汇系统的时空演化记录了印支地块的运动和印度板块与欧亚板块的碰撞。然而，由于复杂的构造运动和地形地貌演化，对盆外物源和盆内物源沉积物的时空分布一直存在争议。本文结合多种资料，回顾了南海西北地区始新世至中新世源汇系统的演化过程。其主要包括初始裂陷阶段、后裂陷阶段和热沉降阶段。首先，我们利用地震剖面解释确定了主要的沉积路径。基于地震资料、岩心样品和粒度分析，重建了沉积区的沉积分布和岩相组合。基于物质平衡计算模型，定量研究了泥沙通量和流域面积。在此基础上，通过对南海北西海域陆相地块基岩、南海新生代基底和河流进行稀土元素(REE)和锆石 U-Pb 年龄分析，以及重矿物研究，恢复了物源区，厘定了迁移距离。根据上述研究，确定了源汇系统的三个阶段：(1)始新世为初始裂陷期，南海活跃的裂陷导致了主要的地形变化。北部湾盆地和莺歌海盆地注入了大量自生滑塌沉积物和少量古红河沉积物。2)渐新世为后裂陷期。区域隆升和构造反转可能与印支地块的顺时针旋转有关，破坏了北部湾盆地与红河流域的联系。古 Qin 河和古 Lian (Nanliu) 河从华夏地块向北部湾盆地注入大量碎屑物质。3)中新世为热沉降阶段，地形向东倾斜增强，流域盆地进入后裂陷阶段。古红河及其支流 Lam 河、Ma 河的发育，将远端沉积物注入莺歌海盆地，而华夏地块以西的河流将沉积物注入北部湾盆地。对源汇系统参数的统计分析表明，始新世时期平均地形高度对沉积区起主导作用，渐新世和中新世时期的主导作用则转为沉积物供应的多少。

ABSTRACT: The northwestern South China Sea (NW-SCS) presents a spatial-temporal evolution of its source-to-sink (S2S) system, that recorded the movement of the Indochina block and the collision between the Indian and Eurasian plates. However, complex tectonic movements and

topographic evolution have led to controversial studies about the spatial-temporal distribution of allogenic materials and autogenic sediments. In this study, we integrated a number of multiscale data to review the S2S system evolution of the northwestern area of the South China Sea from the Eocene to the Miocene. The series include the initial synrift, postrift and thermal subsidence stages. First, we identified the major sediment pathways using seismic profile interpretation. We reconstructed the sediment distribution and lithofacies association within the dispersal sink area based on seismic data, core samples and grain-size analysis. We quantitatively studied the sediment flux and catchment area based on mass balance calculation modeling. Following this, we acquired rare-earth element (REE) data and zircon U–Pb age data from the bedrocks of the continental blocks and the South China Sea Cenozoic basement and rivers in the NW-SCS area to restore the provenance area and evaluate the migration distance by inspecting the heavy mineral assemblages. According to the above studies, three phases of S2S dynamics were identified. 1) The initial rifting stage occurred during the Eocene, and active rifting in the South China Sea induced a major topographic change. A large amount of autogenic slump sediments and a smaller amount of paleo-Red River sediments were injected into the Beibu Gulf Basin (BBGB) and the Yinggehai-Song Hong Basin (YGHB). 2) The postrift stage occurred during the Oligocene. Regional uplift and tectonic inversion probably linked to the clockwise rotation of the Indochina Block, broke the connection between the Beibu Gulf Basin and the Red River catchments. The paleo-Qin River and the paleo-Lian (Nanliu) River brought a large amount of clastic material into the Beibu Gulf Basin from the Cathaysia Block. 3) The thermal subsidence stage occurred during the Miocene: the eastward topographic tilt was enhanced, and the drainage basin entered postrift stage. The development of the Paleo-Red River and its branches, the Lam River and the Ma River, brought distal sediment into the YGHB, while the rivers in the west Cathaysia Block transported sediment into the BBGB. Statistical analysis of the S2S system parameters suggests that the average terrain altitude played a dominant role in determining the S2S system volume during the Eocene, while the dominant role transferred to the sediment supply during the Oligocene and Miocene.

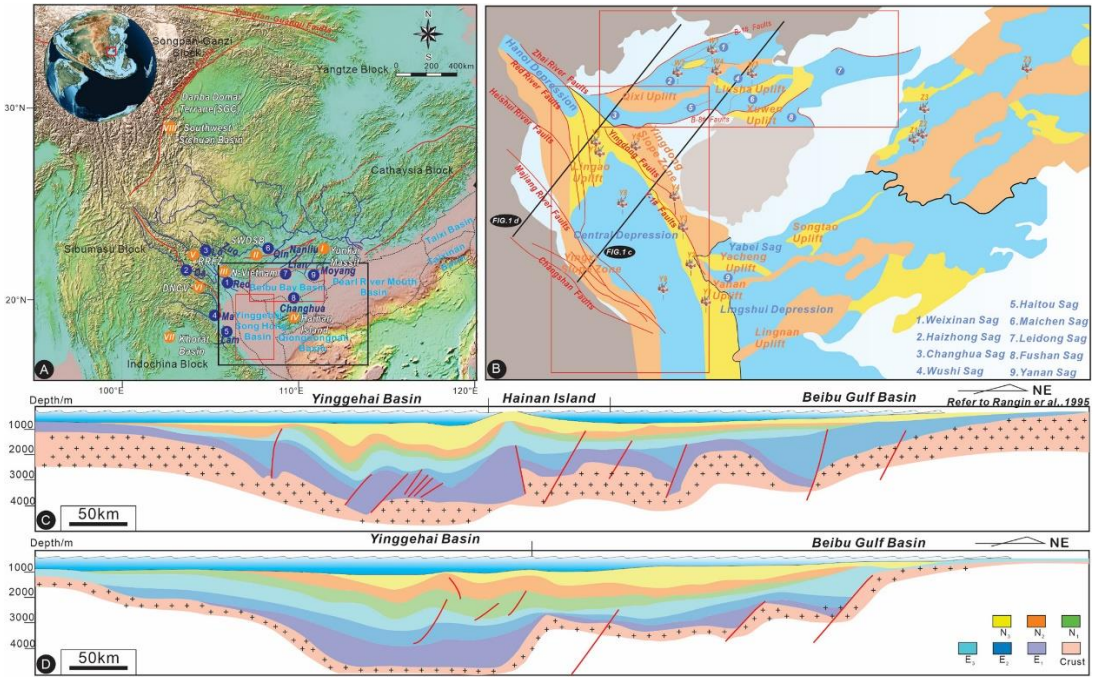

Figure 1. A present the location of the rivers and the tectonic blocks around the NW-SCS. In a clockwise direction, the river named the Pearl River (in Chinese called Zhujiang) and its tributaries are shown: The Moyang River, Lian River (also called Nanliu River), Qin River, Red River and its tributaries, the Ma River, Lam River and Changhua River on Hainan Island. B shows the tectonic division map of the NW-SCS. The yellow bend indicates the uplift area, and the blue bend shows the subsidence area during the Paleogene. The NW-SCS can be divided into two large drainage basins, namely, the Beibu Gulf Basin and the Yinggehai-Song Hong Basin. Modified from the study by Rangin et al. (1995), C and D are two profiles that cross the NW-SCS and show how the strata developed since the Cretaceous period.

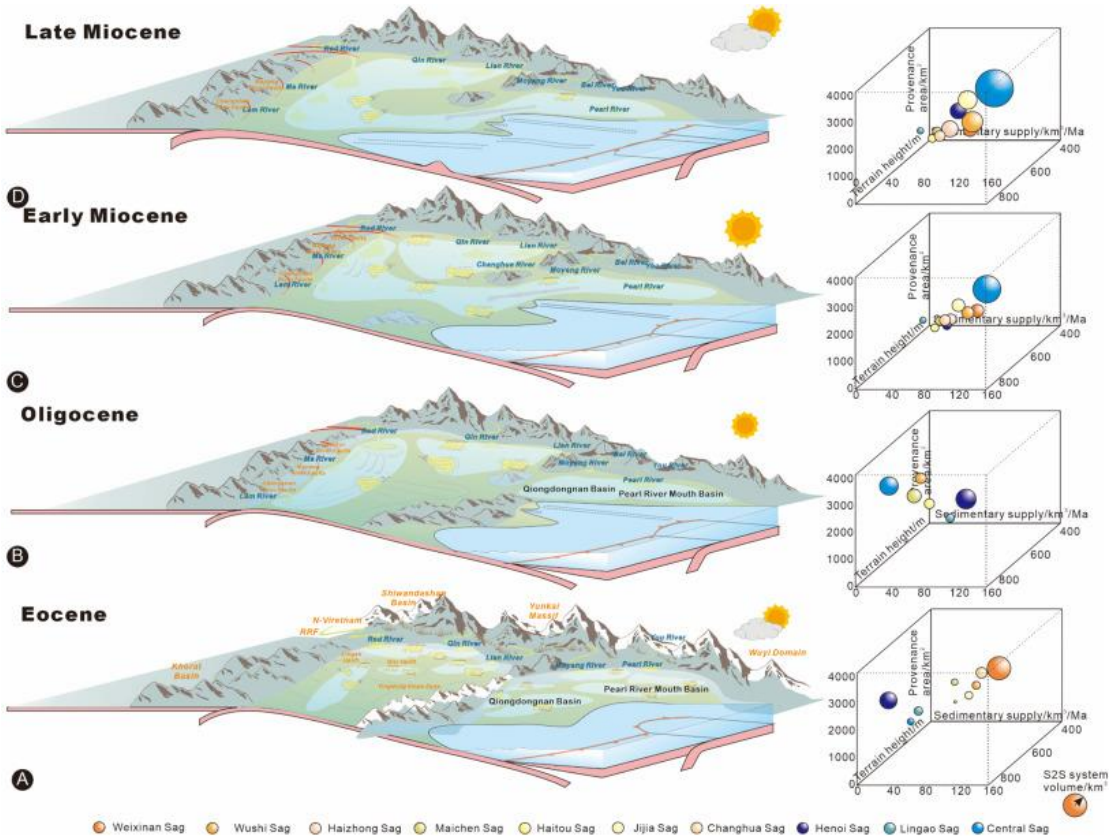

Figure 2. Envisaged paleogeographic evolution of the NW-SCS drainage basin from the rifting stage (Eocene and Oligocene) to the postrifting stage (Miocene) (Panels A to D; based on Maruyama et al., 1997; Fyhn et al., 2020; He et al., 2020). We plotted the S2S parameters in a bubble chart. During the Eocene (A), the fitting equation is $V = 0.04A + 0.05Qs + 0.6e^{H} + 0.5$, $R^2 = 0.46$, where V is the volume of the sink, Qs is the sediment supply, A is the provenance area, H is the relative height of the pathway, and a, b, and c are the fitting coefficients. In the Oligocene (B), we obtain the fitting equation that $V = 0.03H + 0.5A \cdot e^{Qs} + 0.8$, $R_2 = 0.55$. In the early Miocene and the late Miocene, the bubble chart shows a similar pattern, and we combine them together and obtain the fitting equation: $V = 0.2A \cdot H + 0.08 \ln(Qs) + 1.8$, $R_2 = 0.76$.

3. 基于孟加拉湾多指标记录重建的 140-70ka 的印度夏季风变化

翻译人：杨会会 11849590@mail.sustech.edu.cn

Nilssson-Kerr K, Anand P, Sexton P F, et al., ***Indian Summer Monsoon variability 140-70 thousand years ago based on multi-proxy records from the Bay of Bengal [J].*** *Quaternary Science Reviews, 2022, 279, 107403*

https://doi.org/10.1016/j.quascirev.2022.107403

摘要：了解印度夏季风(ISM)在更新世晚期的行为，很大程度上是基于阿拉伯海的“风”驱动的上升流记录。然而，目前还不清楚这些记录在多大程度上也可以用来推断伴随“风”而来的季风降雨，或者说 ISM 的两个组成部分，“风”和“雨”在千年尺度上是如何联系在一起的。为了分离 ISM 降水的主要信号，我们在孟加拉湾北部和安达曼海钻取了两个深海沉积物岩芯(U1446 孔)和 (U1448 孔)，这两个孔都位于南亚大陆的近端，因此，它位于捕获 ISM 降雨和河流径流的理想位置。通过将我们的多指标 ISM 降雨和径流记录与阿拉伯海已发布的 ISM 风驱动记录进行比较，我们发现，在深海氧同位素 5/6 阶段(约 140-70ka BP)，ISM 的“风”和“雨”两个成分明显分离。我们揭示了季风的气压动力(风)和热力(雨)组分的相对优势随着背景气候状态的变化而变化。这一发现对于解释过去的季风重建是一个重要的考虑因素。通过将我们新的 ISM 降雨记录与高纬度气候记录进行比较，我们表明通过季风从低纬度地区输出的水分，可能在冰川初期为高纬度地区的冰盖增长提供了条件。

ABSTRACT: Understanding the Indian Summer Monsoon (ISM) behavior during the late Pleistocene has been largely based on the wind-driven upwelling records from the Arabian Sea. However, it remains unclear the extent to which these records can also be used to infer a concomitant signal of monsoon rainfall, or how the two ISM components, rainfall and wind, are linked on millennial timescales. In order to isolate a primary signal of ISM rainfall, we exploit two deep sea sediment cores from the northern Bay of Bengal (Site U1446) and Andaman Sea (Site U1448), both situated proximal to the South Asian continent, and thus ideally situated for capturing ISM rainfall

and fluvial runoff. By comparing our multi-proxy ISM rainfall and runoff records with published ISM wind-driven records from the Arabian Sea, we observe pronounced decoupling of the rainfall and wind components of the ISM across Marine Isotope Stage 5/6 (~140-70 thousand years ago). We reveal that the relative dominance of barometric dynamics (wind) and the thermodynamic (rainfall) components of the monsoon shifts with changes in background climate state. This finding constitutes an important consideration for the interpretation of past monsoon reconstructions. By comparing our new ISM rainfall records with high latitude climate records, we show that moisture export from low-latitudes, via the monsoon, could have preconditioned the high latitudes for ice sheet growth during glacial inceptions.

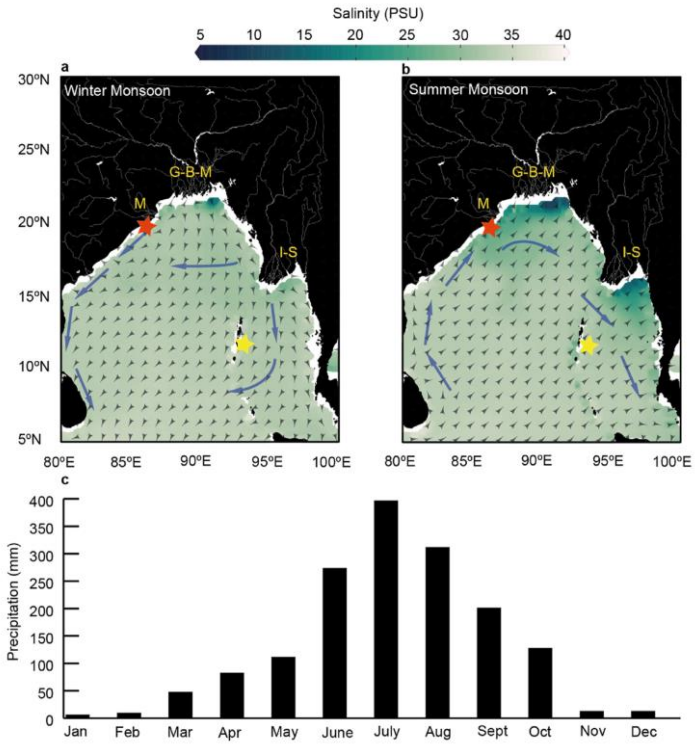

Figure 1. Map of study locations; Site U1446 (red star) and Site U1448 (yellow star). Average monthly sea surface salinity from 2017 for a) winter monsoon months of December-February and b) ISM months June-September (Meissner et al., 2018). Major rivers indicated; G-B-M (Ganges-Brahmaputra-Meghna), M (Mahanadi), I-S (Irrawaddy-Salween). Small black arrows indicate mean wind direction (Fernandez-Lopez and Schliep, 2019) and blue arrows indicate general pattern of surface currents and c) Mean monthly precipitation (Schneider et al., 2017). Figure created using

Ocean Data View software (http://odv.awi.de/). PSU; practical salinity units. (For interpretation of the references to color in this figure legend, the reader is referred to the Web version of this article.)

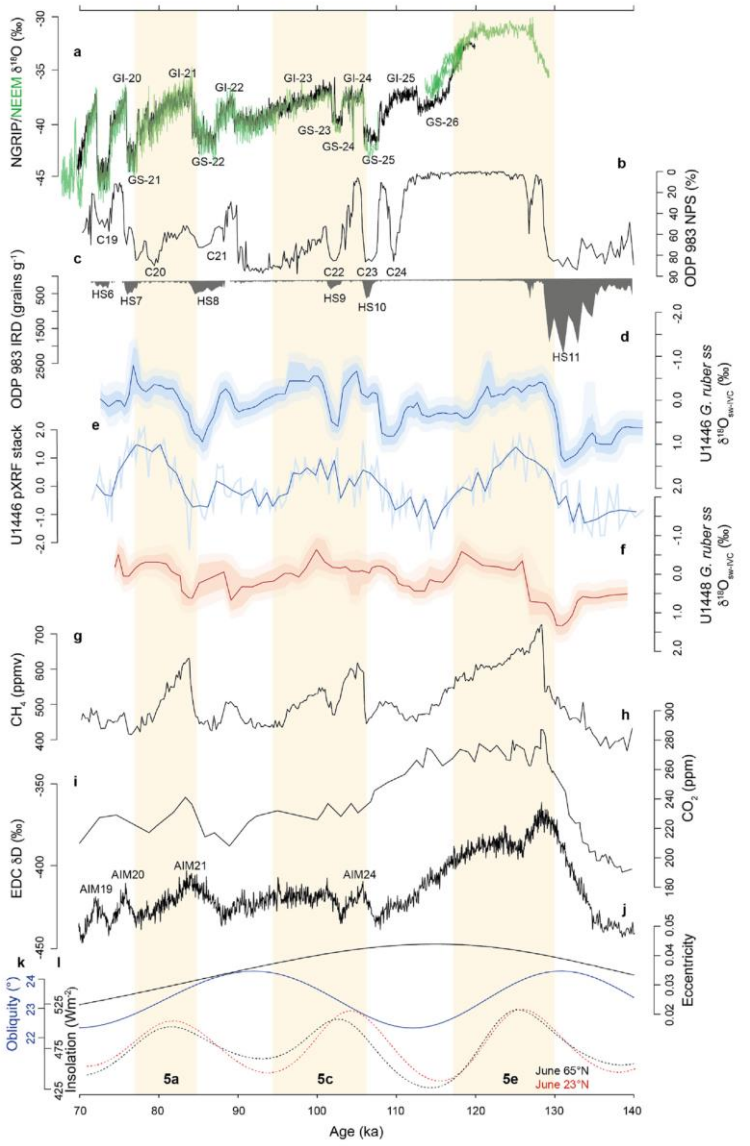

Figure 2. High-latitude and ISM records across MIS 5 a) NGRIP (black) and NEEM (green) ice-core $\delta^{18}O$ (Andersen et al., 2004; Gkinis et al., 2021) b) ODP 983, North Atlantic *Neogloboquadrina pachyderma* (sinistral) % (Barker et al., 2015) c) ODP 983 IRD (grains g^{-1}) (Barker et al., 2015) d) Site U1446 G. *ruber ss* $\delta^{18}O_{sw\text{-}IVC}$ (this study) e) Site U1446 pXRF stack (this study) f) Site U1448 G. *ruber ss* $\delta^{18}O_{sw\text{-}IVC}$ (this study) g) EDC ice-core CH_4 (Loulergue et al., 2008) h) Antarctic composite CO_2 ice-core record (Lüthi et al., 2008) i) EDC icecore δD (Jouzel et al., 2007) j) Eccentricity (Laskar et al., 2004) k) Obliquity (Laskar et al., 2004) and l) 21st June NHSI at 65°N and 23°N (Laskar et al., 2004). All records are on the AICC2012 chronology (Bazin et al., 2013;

Veres et al., 2013). (For interpretation of the references to colour in this figure legend, the reader is referred to the Web version of this article.)

4. 海相碳酸盐岩缓冲作用下俯冲的有机质主导了岛弧排放 CO_2 的碳同位素特征

翻译人：王敦繁 Dunfan-w@foxmail.com

Tumiati, S., Recchia, S., Remusat, L. et al. ***Subducted organic matter buffered by marine carbonate rules the carbon isotopic signature of arc emissions[J]****. Nature Communications, 2022; 13, 2909 https://doi.org/10.1038/s41467-022-30421-5*

摘要：海洋沉积物主要由碳酸钙和有机物(浮游植物碎屑)组成。一旦俯冲，一些碳就会从板块中移除，以二氧化碳的形式回到大气中。其同位素特征被认为反映了沉积源中无机(碳酸盐)碳和有机(石墨)碳的分馏。这里，我们通过对由 ^{13}C-$CaCO_3$ + ^{12}C -石墨组成模型的沉积物在压力、温度和氧化还原条件下在弧下平均板幔界面与水相互作用的研究来验证这一假设。结果表明，石墨氧化溶解是控制 CO_2 生成的主要过程，其同位素组成反映的是 CO_2/$CaCO_3$，而不是整体石墨与 $CaCO_3$(即有机/无机碳)组分对比值。本文还建立了弧源流体-岩石 CO_2 同位素的特征信号与俯冲过程中的氧化还原状态之间的数学模型。

ABSTRACT: Ocean sediments consist mainly of calcium carbonate and organic matter (phytoplankton debris). Once subducted, some carbon is removed from the slab and returns to the atmosphere as CO_2 in arc magmas. Its isotopic signature is thought to reflect the bulk fraction of inorganic (carbonate) and organic (graphitic) carbon in the sedimentary source. Here we challenge this assumption by experimentally investigating model sediments composed of ^{13}C-$CaCO_3$ + ^{12}C-graphite interacting with water at pressure, temperature and redox conditions of an average slab–mantle interface beneath arcs. We show that oxidative dissolution of graphite is the main process controlling the production of CO_2, and its isotopic composition reflects the CO_2/$CaCO_3$ rather than the bulk graphite/$CaCO_3$ (i.e., organic/inorganic carbon) fraction. We provide a mathematical model to relate the arc CO_2 isotopic signature with the fluid–rock ratios and the redox state in force in its subarc source.

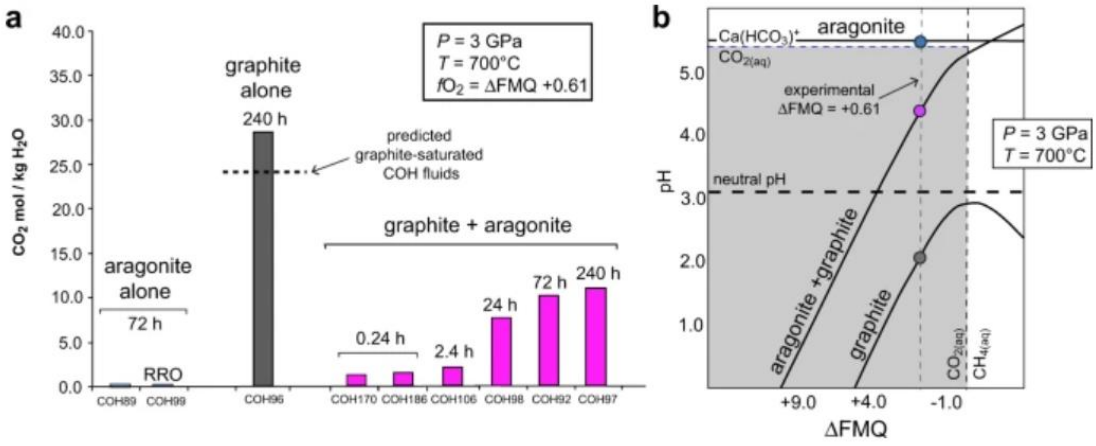

Figure 1. a) CO_2 concentration (molality) in experimental aqueous fluids interacting with (i) aragonite-only (blue), (ii) graphite-only (grey) and (iii) graphite + aragonite (magenta). Typical analytical uncertainty is 1 mol%. Dashed line: CO_2 content predicted by thermodynamic modelling of graphite-saturated COH fluids. Run duration (h) is shown at the top of each bar. RRO: run buffered by Re–ReO_2 (ΔFMQ $\approx$ +2) instead of ferrosilite + magnetite + coesite; b) fO_2 vs. pH diagram at 3 GPa and 700 °C generated by thermodynamic modelling (Deep Earth Water model[26,28]) of aqueous fluids in equilibrium with aragonite-only (blue dot), graphite-only (grey dot) and aragonite + graphite (magenta dot). Black solid lines: saturation curves. Coloured dots: experimental conditions at fO_2 buffered by ferrosilite + magnetite + coesite. Grey field: $CO_{2(aq)}$ is the dominant carbon-bearing species; it is adjacent to $Ca(HCO_3)$+-dominated field at higher pH and to $CH_{4(aq)}$-dominated field at lower fO_2 values. Neutral pH is shown for reference with a dashed line. Calculations are performed at 3 GPa, 700 °C and fH_2 buffered by ferrosilite + magnetite + coesite + H_2O (equivalent to log (fO_2 /1 bar)= −13.36; ΔFMQ = +0.61).

5. 印度洋沉积碳酸钙分布及其对冰期深海环流的意义

翻译人：曹伟 11930854@qq.com

Zhang H D, Luo Y M, Yu J., et al. ***Indian Ocean sedimentary calcium carbonate distribution and its implications for the glacial deep ocean circulation Estimating*** *[J]. Quaternary Science Reviews, 2022, 184:107490*

https://doi.org/10.1016/j.quascirev.2022.107490

摘要：通过大气和海洋之间的碳交换调节大气中的二氧化碳，海洋在全球气候中发挥着关键作用，这一过程与海洋环流变化密切相关。海洋环流通过深水形成将大气中的 CO_2 输送到深海，然后通过释放 CO_2 进行转换，从而调节海底海洋沉积物中 $CaCO_3$ 的积累。相比于大西洋和太平洋的研究，对印度洋过去环流变化的研究要少得多。这在一定程度上是由于缺乏对次海盆尺度碳酸钙 ($CaCO_3$)分布的系统研究，以及对其在印度洋的控制机制的了解有限。基于广泛的数据汇总和简单的碳酸盐累积模型，本研究表明印度洋各盆地的 $CaCO_3$ 分布主要受海洋环流变化的控制，生产力仅起次要作用。末次盛冰期 (LGM) 和晚全新世之间 $CaCO_3$ 分布的对比表明，这些时期深水酸度变化不大。如果水源酸度随着时间的推移保持不变，这一发现表明在 LGM 期间印度洋深部有强烈的通量。鉴于冰川海洋可能更具碱性，印度深部酸度的稳定性强烈表明在 LGM 期间碳（主要作为碳酸氢根离子）的储存量更大。此外，我们在西南印度盆地发现了一种腐蚀性很强的 LGM 深水，这可能归因于太平洋深水的侵入。

ABSTRACT: The ocean plays a critical role in the global climate by modulating atmospheric CO_2 via carbon exchange between the atmosphere and the ocean, a process tightly linked to ocean circulation changes. Ocean circulation transports atmospheric CO_2 to the deep ocean via deep water formation and then transfers it with respired CO_2, which regulate $CaCO_3$ accumulation in marine sediments on seafloor. Compared to studies on the Atlantic and Pacific, much less has been done on past circulation changes in the Indian Ocean. This is partly due to the lack of systematic investigation on sub-basinal scales calcium carbonate ($CaCO_3$) distributions and limited

understanding of their controlling mechanisms in the Indian Ocean. Based on an extensive data compilation and a simple carbonate accumulation model, here we show that $CaCO_3$ distributions in various basins of the Indian Ocean are mainly controlled by ocean circulation changes with productivity only playing a secondary role. Comparison of $CaCO_3$ distributions between the Last Glacial Maximum (LGM) and the late Holocene suggests little change in deep water acidity between these times. If the source-water acidity remains unchanged through time, this finding suggests a vigorous ventilation of the deep Indian Ocean during the LGM. Given that the glacial oceans were likely more alkaline, the stability of deep Indian acidity must suggest greater storage of carbon (mainly as bicarbonate ion) during the LGM. Additionally, we find a very corrosive LGM deep water in the Southwest Indian Basin which may be attributed to intrusion of the Pacific Deep Water.

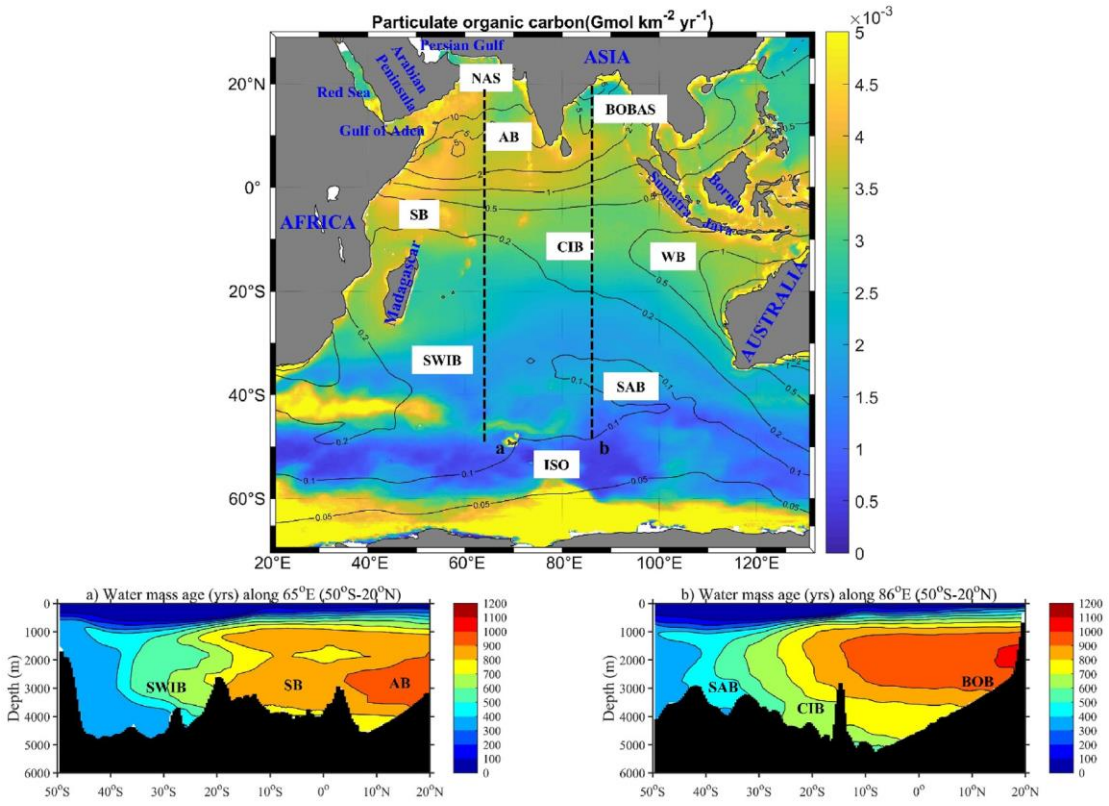

Figure 1. *Annual export of particulate organic carbon (POC) (shading) and dust (contours) fluxes in the Indian Ocean.*

6. 过去 244 kyrs 期间，海平面变化和黑潮入侵主导了南海东北部台湾沉积物的源-汇过程

翻译人：王浩森 11930841@mail.sustech.edu.cn

Zhang, C., Yang, S., Huang, X., Dou, Y., Li, F., Xu, X., Hao, Q., Gao, J., 2022. ***Sea level change and Kuroshio intrusion dominated Taiwan sediment source-to-sink processes in the northeastern South China Sea over the past 244 kyrs****. Quaternary Science Reviews, 287, 107558.*

https://doi.org/10.1016/j.quascirev.2022.107558

摘要：大陆边缘陆源沉积物源-汇过程由气候、输沙量、海平面和海洋环流在不同时空尺度上的复杂的相互作用决定。由于晚第四纪以来，南海东北部（NSCS）边缘大量陆源沉积物的输入和连续沉积，可以作为一个天然实验室来探究这些过程。根据 NSCS 陆坡长 35 m 的沉积层序（MD12-3429 岩芯），我们根据地球化学成分区分了沉积物来源，然后通过各种沉积记录（包括物质累积率（MAR）、有孔虫数据，粒径端元模型（EMM）和光谱分析。地球化学指标包括常量元素比值和稀土元素分馏参数表明，岩芯中的碎屑沉积物主要来自台湾。陆源沉积物的 MAR 平均值为 9.6 g/cm^2/kyr，在冰期和间冰期都观察到较高的 MAR 值。EMM 结果显示，三个端元模型的主要粒径尺寸分别为 6.6 μm（EM1）、26.3 μm（EM2）和 49 μm（EM3）。最细端元（EM1）和最粗端元（EM3）的时间变化清楚地表明了冰期-间冰期旋回性，光谱分析表明 100 kyr 偏心率占主导地位，这表明海平面变化是 NSCS 大陆边缘沉积的一级控制。此外，随着东亚季风的减弱，水动力敏感分量（EM2）及其 MAR 的时间变化呈现逐渐增大的趋势。结合现代观测和模拟结果，我们认为，黑潮入侵增强可能是晚第四纪台湾沉积物运移的原因。正如 EM2 中 31 kyr 的周期性所示，我们推断，类厄尔尼诺现象的发展加强了来自吕宋海峡的黑潮的入侵，导致台湾陆源 MAR 明显增加，但南海东北部的初级生产力下降。本研究深入了解了晚第四纪快速变化的边缘海环境中复杂的陆源沉积物源-汇过程。

ABSTRACT: The terrigenous sediment source-to-sink processes in continental margins are determined by complex interactions among climate, sediment discharge, sea level and oceanic

circulations on various temporal and spatial scales. The northeastern South China Sea (NSCS) margin is a natural laboratory to catch a glimpse of these processes due to large amounts of terrigenous sediment inputs and continuous sedimentations during the late Quaternary. Based on a 35 m-long sedimentary sequence (core MD12-3429) retrieved from the NSCS upper continental slope, we distinguished sediment sources based on geochemical compositions, and then linked sedimentary responses to sea level change and Kuroshio intrusion over the past 244 kyrs via various sedimentary records including mass accumulation rates (MAR), foraminifera data, grain-size end-member modeling (EMM) and spectral analysis. Geochemical proxies including major element ratios and fractionation parameters of rare earth elements suggest that the detrital sediment in the core was derived primarily from the Taiwan. The MAR of terrigenous sediment yields an average 9.6 g/cm^2/kyr, and high MAR values are both observed in glacial and interglacial intervals. The results of EMM reveal three end-members with dominant modal grain sizes of 6.6 μm (EM1), 26.3 μm (EM2) and 49 μm (EM3), respectively. The temporal variations of the finest end-member (EM1) and the coarsest end-member (EM3) demonstrate clearly glacial-interglacial cyclicity, and the spectral analysis indicates the dominance of 100-kyr eccentricity, which suggests that sea level changes are the first-order control for the NSCS continental margin sedimentation. In addition, the temporal variations in hydrodynamic sensitive component (EM2) and its MAR display gradually increasing trends with weakening East Asian monsoon. Combing with modern observation and modeling results, we suggest that enhanced Kuroshio intrusion might account for the transport of Taiwan-derived sediment during the late Quaternary. As indicated by a 31 kyr periodicity in EM2, we infer that the development of El Niño-like condition strengthened the intrusion of oligotrophic Kuroshio from the Luzon Strait, resulting in the obvious increase of Taiwan terrigenous MAR but decreases of the primary productivity in the northeastern South China Sea. This study provides deep insight into the complex terrigenous sediment source-to-sink processes in a fast-changing marginal sea environment during the late Quaternary.

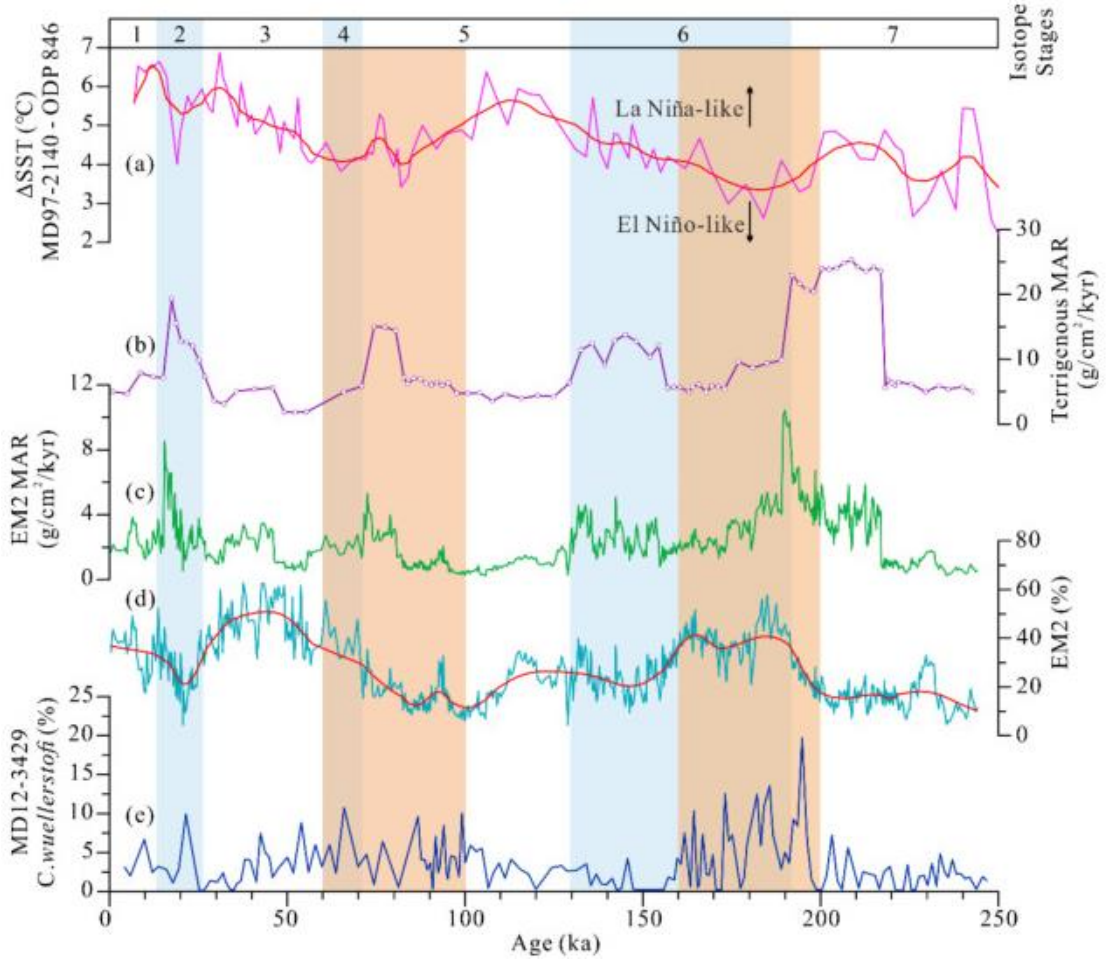

Figure 1. Temporal variations in EM2 abundance and MAR and their comparisons to other proxies. (a) ΔSST between core MD97-2140 and core ODP Site 846. (b) Terrigenous MAR of core MD12-3429. (c) Terrigenous MAR of EM2. (d) Variations of EM2 abundances. (e) Variations of benthic foraminifera *C. wuellerstorfi* content (%) in core MD12-3429. The data of ΔSST (a) were smoothed by a 3-point Fast Fourier Transform (FFT) filter, and the EM2 abundances (d) were smoothed by a 20-point FFT filter. Two shallow orange shadings highlight the periods of enhancing El Niño-like conditions.

7. 贵州中部瓜德鲁普统硅质沉积地层:中二叠世生物危机时期碳酸盐岩生产力的区域相关性

翻译人：张伟杰 12031188@mail.sustech.edu.cn

Meng Q, Xue W, Chen F, et al. ***Stratigraphy of the Guadalupian (Permian) siliceous deposits from central Guizhou of South China: Regional correlations with implications for carbonate productivity during the Middle Permian biocrisis****[J]. Earth-Science Reviews, 2022, 228: 104011. https://doi.org/10.1016/j.earscirev.2022.104011*

摘要：与二叠纪末生物大灭绝的大量研究相比，尽管瓜德鲁普世生物大灭绝标志着与全球环境变化相关的重大生物更替，但相关研究很少。在该事件中，中国南方礁质碳酸盐岩停止生成，被富硅质、富泥沉积（SRDs）所取代。然而，这一时期碳酸盐岩台地生产力的变化仍有待进一步研究。本文对贵州中部扬子碳酸盐岩台地上发育的瓜德鲁普统 SRDs 进行了沉积学和牙形石生物地层研究。在瓜德鲁普统层序与华南地层对比的基础上，研究结果表明，样子碳酸盐台地的完整性与台地构造演化不匹配。台地演化过程中出现了台地内坳陷以及 SRDs 在台地边缘逐渐叠加。地层对比表明，台地在早罗德期、晚沃德期和晚卡皮敦期经历了 3 个阶段的 SRDs 叠加。台地碳酸盐岩在前两阶段后重新扩展，但在最后阶段没有扩展。本文提出了瓜德鲁普世碳酸盐岩台地的演化模式，该模式遵循同时期海平面升降波动。台地边缘的逐渐后撤可能表明瓜德鲁普世台地顶部碳酸盐沉积物供应不足。碳酸盐岩生产力的变化引起了人们对浅水碳酸盐岩工厂变化的关注，这与瓜德鲁普世分泌碳酸盐岩生物群的命运以及影响碳酸盐岩台地生产者的环境因素密切相关。

ABSTRACT: In comparison with the amount of study undertaken on the end-Permian mass extinction, the preceding Guadalupian mass extinction has received little investigation, even though it marks a significant biotic turnover associated with global environmental changes. During the earlier event, reef carbonate production shut down and was replaced by siliceous, mud-rich deposits (SRDs) in South China. However, changes in carbonate platform productivity during this epoch remain to be clarified. This paper presents sedimentological and conodont biostratigraphic investigations on the Guadalupian SRDs developed on the Yangtze Carbonate Platform (YCP) in

central Guizhou. The findings are viewed in the context of Guadalupian sequence correlation of South China successions, which shows that the integrity of the YCP failed to match the platform tectonic evolution. The platform evolution saw the onset of major intra-platform depressions and the gradual onlap by SRDs along the platform margin. Stratigraphic correlation reveals that the platform experienced three phases of onlap by SRDs during the early Roadian, the late Wordian and the late Capitanian upwards. Platform carbonates re-expanded their extent following the first two phases, but not during the final phase. An evolutionary model is proposed for the Guadalupian carbonate platform, which follows the contemporaneous eustatic sea-level fluctuations. The partial drowning observed within the platform interior and increasing retreat along the platform margin could suggest an insufficient carbonate sediment supply shedding from the platform top during the Guadalupian. The variation in carbonate productivity raises our attention to the change in shallow-water carbonate factories, which is closely related to the fortunes of carbonate-secreting biota and environmental factors impacting the carbonate platform producers during the Guadalupian.

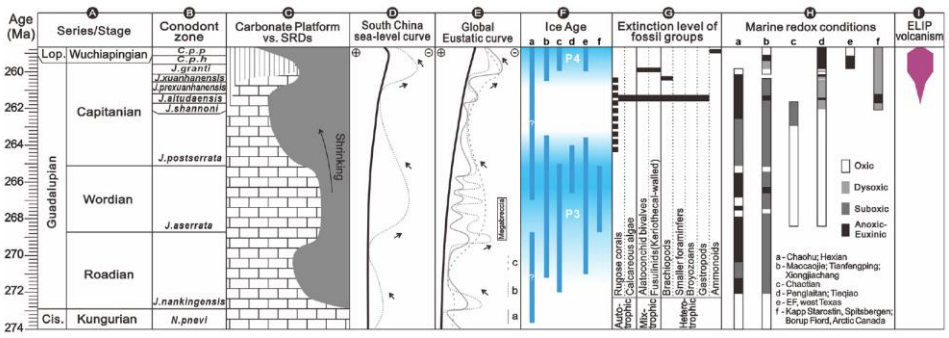

Figure 1. Summary on the evolution of carbonate platforms in South China and possible influencing factors during the Middle-Late Permian. (A, B) Timescale and biostratigraphic framework from Henderson (2016) and Shen et al. (2018). (C) Generalized platform margin onlaps based on this study. The interval filled by vertical lines shows missing strata caused by regression. (D) South China relative sea-level changes modified from Wang et al. (1999). (E) Global eustatic sea-level changes modified from: a - Haq and Schutter (2008); b - Ross and Ross (1987); c - Haq and Al-Qahtani (2005). Megabreccia event from Haq and Schutter (2008). (F) Durations of glacial events. Data of a-d are from eastern Australia and recalibrated in this timescale based on: a - Fielding et al. (2008); b - Metcalfe et al. (2015); c - Frank et al. (2015); d - Garbelli et al. (2019). Data of e and f are from: e - NE Russia (Davydov et al., 2016; Davydov et al., 2018b); f - Arctic Canada

(Beauchamp and Grasby, 2012). (G) Extinction levels of different fossil groups summarized from Wang and Sugiyama (2001), Weidlich (2002a), Ota and Isozaki (2006), Isozaki and Aljinovi´c (2009), Shen and Shi (2009), Bond et al. (2010a) and Huang et al. (2018). (H) Comparison of marine redox conditions in: a - central Anhui (Wei et al., 2019; Zhang et al., 2019a); b - western Hubei (Shi et al., 2016; Wei et al., 2016) and central Guizhou (Wignall et al., 2009a); c - northern Sichuan (Saitoh et al., 2013b); d – central Guangxi (Zhang et al., 2015; Wei et al., 2016); e - West Texas (Zhang et al., 2015); f - Spitsbergen and Arctic Canada (Bond et al., 2015; Bond et al., 2019). (I) Volcanism of the ELIP from Sun et al. (2010) and Wu et al. (2020).

8. 与 17 世纪中期火山喷发相对应的气候、天气和社会经济条件

翻译人：李海 12031330@mail.sustech.edu.cn

Stoffel M, Corona C, Ludlow F, et al. ***Climatic, weather and socio-economic conditions corresponding with the mid-17th century eruption cluster*** *[J]. Climate of the Past, 2021: 1-48. https://doi.org/10.5194/cp-18-1083-2022*

摘要：17 世纪中期的特点是，17 世纪 30、40 年代爆发了一系列火山爆发，气候条件在蒙德极小期达到顶峰，西欧、北欧、中国和日本地区的政治动荡和饥荒。本文使用冰芯、树轮和历史证据研究 17 世纪 30、40 年代火山喷发的来源以及它们对当代气候的可能影响，还将研究他们发生的社会政治背景以及可能引发的人类反应。在 1637、1641-1642 和 1646 年的格陵兰冰芯记录中发现了三个不同的硫峰值。在南极洲，只有一次明确的硫酸盐峰值记录（1642 年）。1641-1642 年的双硫峰值可能是由于帕克山火山的喷发，但驹岳火山的喷发也可能导致格陵兰岛观测到硫酸盐峰值。1637 年和 1646 年较小的峰值可能归因于 Hekla 火山和 Shiveluch 火山的喷发。然而，迄今为止，尚未确认 17 世纪中期硫酸盐峰值的火山中没有一个在冰芯中保存有火山灰。树轮和书面资料表明，17 世纪 30 年代末与 40 年代初欧洲各地天气寒冷和歉收。然而，17 世纪早期的另一个特点是欧洲各地爆发了广泛的战争--尤其是“三十年战争”（1618-1648 年）--这使得社会经济危机归咎于火山活动具有挑战性。在中国和日本，历史资料表明，从 1638 年（中国）和 1640 年（日本）发生的极端干旱和饥荒发生在驹岳和帕克山喷发之前。1637-1646 年爆发群的情况以及其后记录的气候和社会条件提供了教科书式的例子，说明了在以下方面的困难：（1）明确区分火山引起的冷却、湿润或干燥与自然气候变化，（2）将政治不稳定、收成歉收和饥荒仅仅是火山气候的影响。这个例子表明，虽然需在当代社会经济背景下研究过去火山活动的影响，现在也是时候抛弃那些将气候视为重大历史事件的重要促成因素的简化框架和有时是反对立场。

ABSTRACT: The mid-17th century is characterized by a cluster of explosive volcanic eruptions in the 1630s and 1640s, climatic conditions culminating in the Maunder Minimum, and political instability and famine in regions of western and northern Europe as well as China and Japan. This

contribution investigates the sources of the eruptions of the 1630s and 1640s and their possible impact on contemporary climate using ice core, tree-ring, and historical evidence but will also look into the socio-political context in which they occurred and the human responses they may have triggered. Three distinct sulfur peaks are found in the Greenland ice core record in 1637, 1641-1642, and 1646. In Antarctica, only one unambiguous sulfate spike is recorded, peaking in 1642. The resulting bipolar sulfur peak in 1641-1642 can likely be ascribed to the eruption of Mount Parker (6° N, Philippines) on 26 December 1640, but sulfate emitted from Komaga-take (42° N, Japan) volcano on 31 July 1641 has potentially also contributed to the sulfate concentrations observed in Greenland at this time. The smaller peaks in 1637 and 1646 can be potentially attributed to the eruptions of Hekla (63°N, Iceland) and Shiveluch (56° N, Russia), respectively. To date, however, none of the candidate volcanoes for the mid-17th century sulfate peaks have been confirmed with tephra preserved in ice cores. Tree-ring and written sources point to cold conditions in the late 1630s and early 1640s in various parts of Europe and to poor harvests. Yet the early 17th century was also characterized by widespread warfare across Europe - and in particular the Thirty Years' War (1618-1648) - rendering any attribution of socio-economic crisis to volcanism challenging. In China and Japan, historical sources point to extreme droughts and famines starting in 1638 (China) and 1640 (Japan), thereby preceding the eruptions of Komaga-take (31 July 1640) and Mount Parker (4 January 1641). The case of the eruption cluster between 1637 and 1646 and the climatic and societal conditions recorded in its aftermath thus offer a textbook example of difficulties in (i) unambiguously distinguishing volcanically induced cooling, wetting, or drying from natural climate variability and (ii) attributing political instability, harvest failure, and famines solely to volcanic climatic impacts. This example shows that while the impacts of past volcanism must always be studied within the contemporary socio-economic contexts, it is also time to move past reductive framings and sometimes reactionary oppositional stances in which climate (and environment more broadly) either is or is not deemed an important contributor to major historical events.

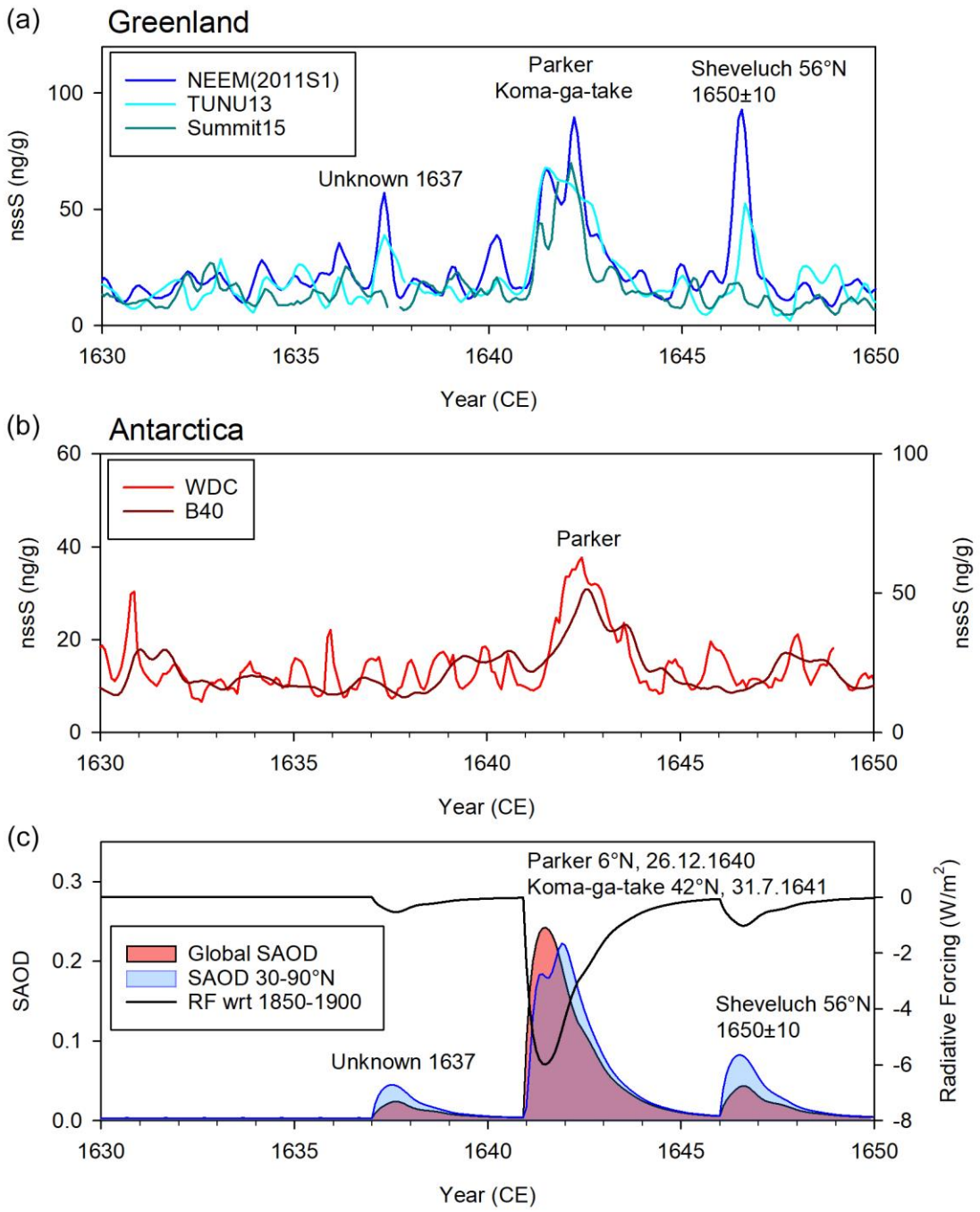

Figure 1. Monthly resolution non-sea-salt sulfur records from ice cores in (a) Greenland and (b) Antarctica, with (c) stratospheric aerosol optical depth (SAOD) and estimated radiative forcing (RF) between 1630 and 1650 (data: Toohey and Sigl, 2017b).

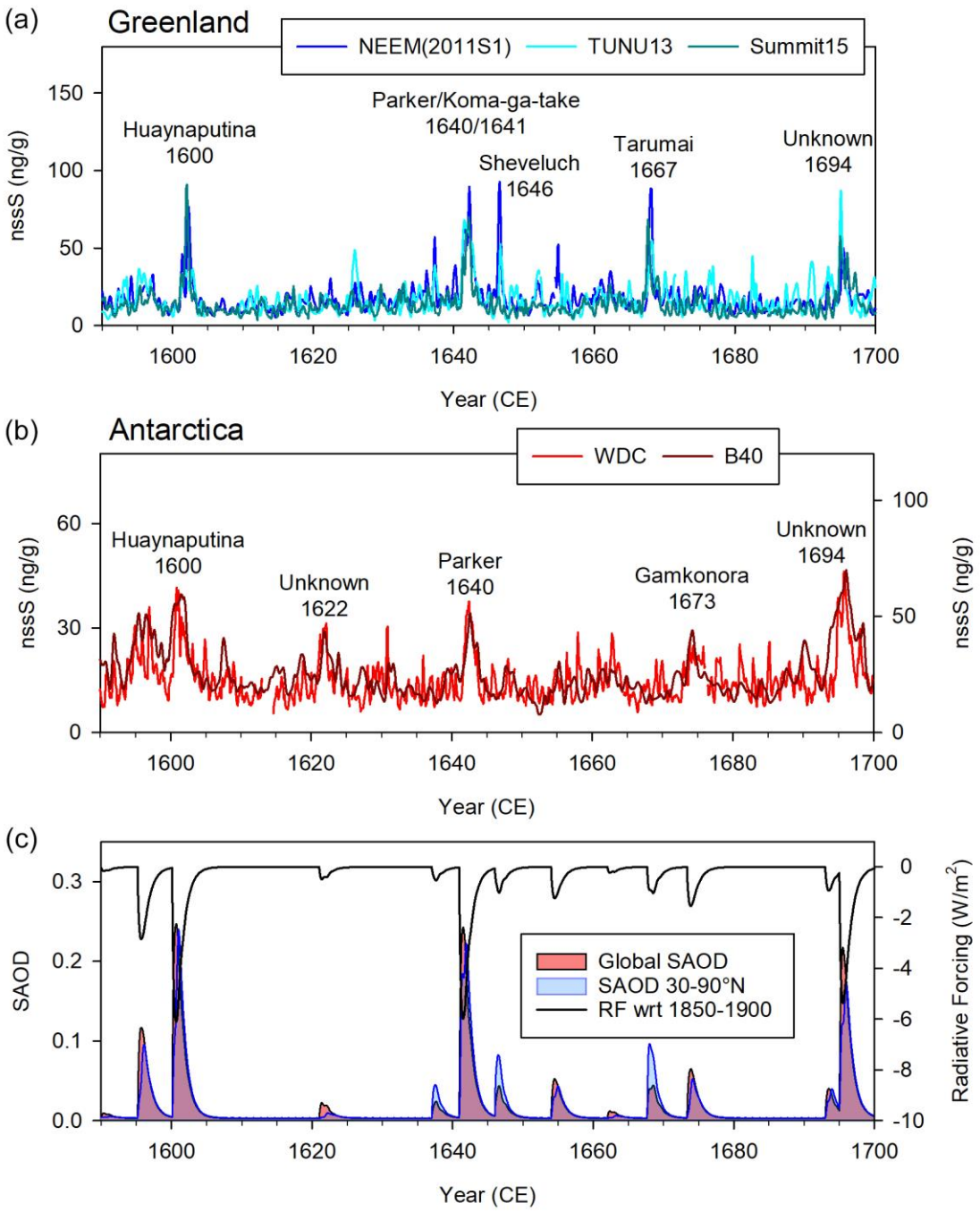

Figure 2. Monthly non-sea-salt sulfur records from ice cores in Greenland and Antarctica, SAOD, and radiative forcing during the 17th century (Toohey and Sigl, 2017b).

9. 深海沉积间断追踪新生代海洋底流的活力

翻译人：张亚南 zhangyn3@mail.sustech.edu.cn

Dutkiewicz A, and Müller R D. ***Deep-sea hiatuses track the vigor of Cenozoic ocean bottom currents*** *[J]. Geology, 2022, 50(6), 710-715.*

https://doi.org/10.1130/G49810.1

摘要：深海沉积中充满了许多间断，这些沉积间断能够追踪海洋环流和化学变化，但由于早期数据的缺乏以及海洋通道演化的认识不全，限制了确定这些间断发生的时间和原因。文中作者将一个扩展的，年龄校准后的深海地层数据库与全球构造和古水深模型结合起来，研究了新生代> 400 个超过~ 0.2 百万年的沉积间断分布。作者发现只有少量的间断是由碳酸盐溶解引起的。大多数的间断是由机械侵蚀和底流对沉积物的改造所引起的。将区域间断发生高峰期与海洋环流和深水形成强度联系一起，南大西洋、南太平洋和南印度洋在大约 30-34 Ma 期间广泛发育的间断是由于德雷克海峡在该时期的扩宽和加深，以及塔斯曼通道的打开。中新世早期大西洋的一次间断高峰期，与德雷克海峡深层通道的完全打开和特提斯海道的逐渐关闭有关，其可能导致了原始大西洋经向翻转环流的形成。14 Ma 以来间断发生频率减少了 30%与 post-Miocene Climate Optimum 的降温是同步的，表明了深海环流的减缓。因此，合成的海洋间断可以用来追踪深海沉积物的演化和约束深海环流模型。

ABSTRACT: The deep-sea stratigraphic record is full of gaps. These hiatuses track changes in ocean circulation and chemistry, but determining their timing and causes has been limited by sparse data and incomplete knowledge of ocean gateway evolution in earlier studies. We combine a significantly expanded, age-calibrated deep-sea stratigraphic database with a global tectonic and paleo–water depth model to investigate the distribution of >400 Cenozoic hiatuses longer than ~0.2 m.y. We find that only a small number of hiatuses are due to carbonate dissolution. The majority of hiatuses were, by implication, caused by mechanical erosion and redistribution of sediments by bottom currents into regions of increased sedimentation such as contourite drifts. We link peaks in regional hiatuses to changes in ocean circulation and intensification of deep-water formation.

Widespread hiatuses in the South Atlantic, South Pacific, and southern Indian oceans between ca. 34 Ma and 30 Ma are attributed to the coeval widening and deepening of the Drake Passage and the opening of the deep Tasman Gateway. A peak in hiatuses in the Atlantic in the early Miocene is linked to the initiation of a proto–Atlantic Meridional Overturning Circulation driven by the complete opening of the deep Drake Passage and the progressive closure of the Tethys seaway. A long-term 30% decline in hiatus frequency since ca. 14 Ma is synchronous with post–Miocene Climate Optimum cooling, suggesting the slowing of abyssal circulation. Our synthesis of deep-sea hiatuses could be used to track the fate of deep-sea sediments and to ground-truth deep-ocean circulation models.

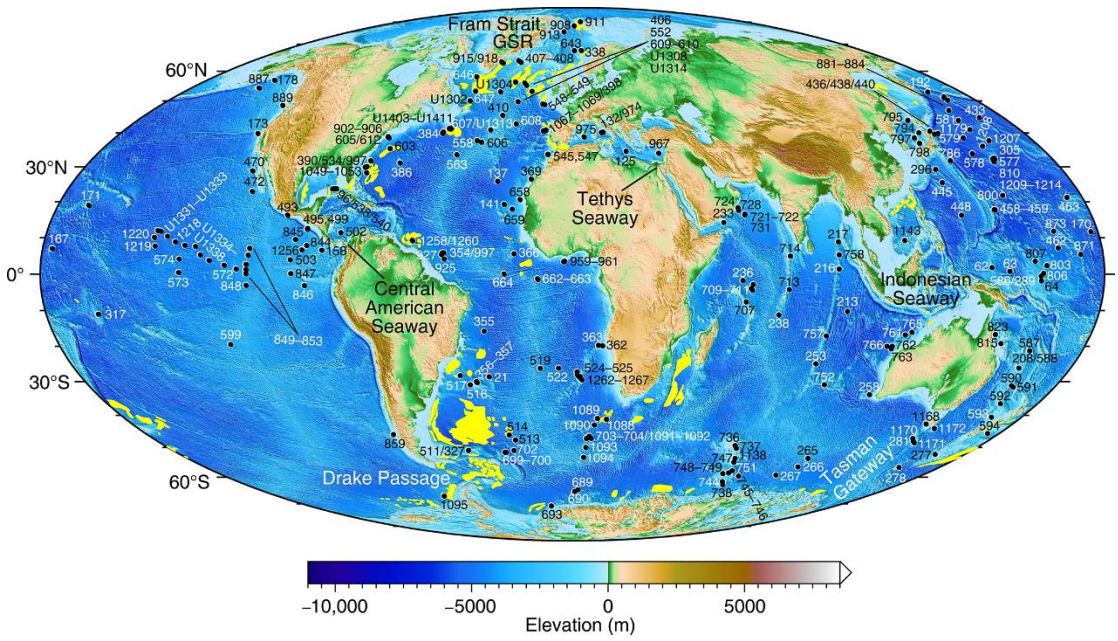

Figure 1. Scientific ocean drilling sites (black circles) of the Deep-Sea Drilling Project (DSDP), Ocean Drilling Program (ODP), Integrated Ocean Drilling Program and the International Ocean Discovery Program used in this study (see the Supplemental Material for a description and access to the data used in this study). Elevation is from ETOPO1 global relief model (https://www.ngdc.noaa.gov/mgg/global/). Contourite drifts in yellow are from Thran et al. (2018). Major ocean gateways are indicated. Mollweide projection. GSR—Greenland-Scotland Ridge.

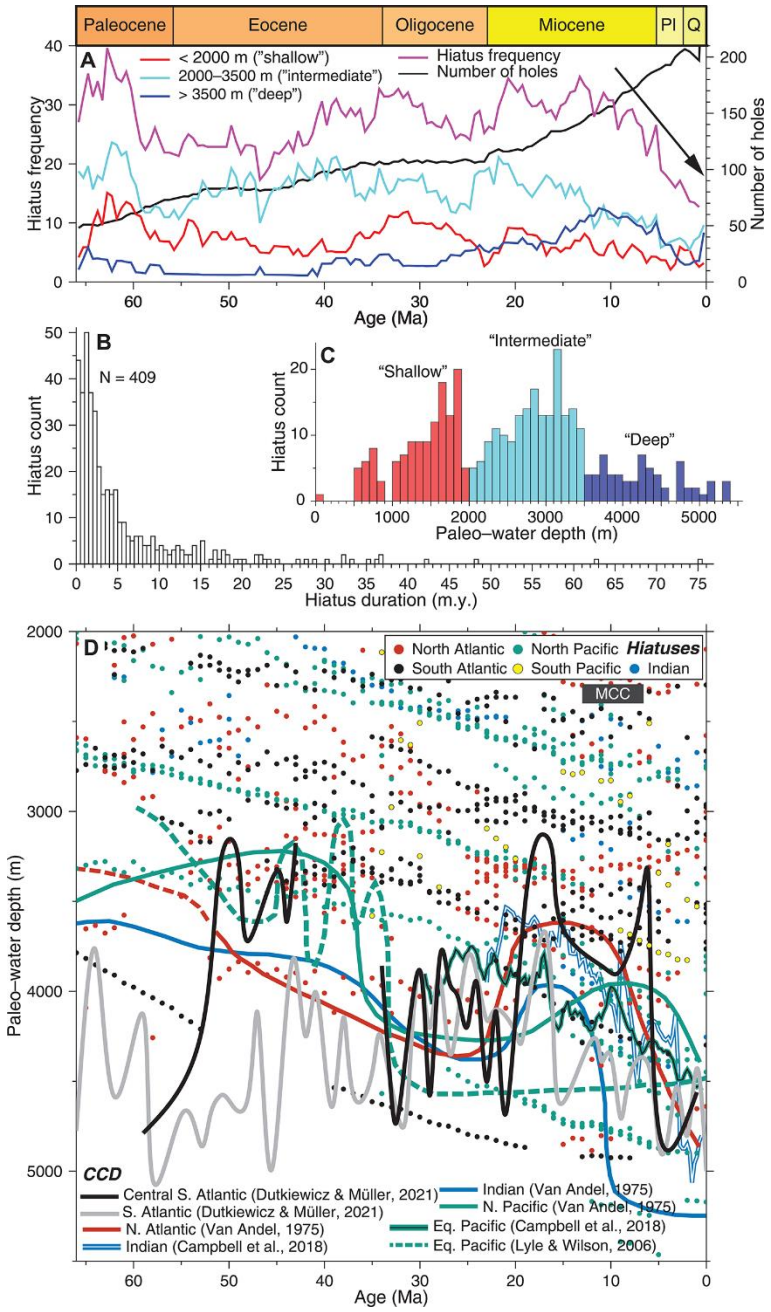

Figure 2. Distribution characteristics of Cenozoic deep-sea hiatuses. (A) Number of drill sites (black) and frequency of global hiatus occurrence (magenta) in 0.5 m.y. bins, subdivided into three paleobathymetric modes in 0.5 m.y. bins: shallow (<2000 m; red), intermediate (2000–3500 m; cyan), and deep (>3500 m; blue). Arrow highlights decreasing trend in hiatus frequency since mid-Miocene. Pl—Pliocene; Q—Quaternary. (B) Histogram of hiatus duration. (C) Trimodal distribution of hiatus paleo–water depths color-coded as in A. (D) Hiatus paleo–water depths and their ages in 0.5 m.y. bins. Paleo–water depths <2000 m are shown in Figure S2 (see footnote 1). Note that relatively few hiatus paleo–water depths occur below regional carbonate compensation

depth (CCD). Timing of Miocene carbonate crash (MCC) is based on compilation of Torfstein and Steinberg (2020). Eq.—equatorial.

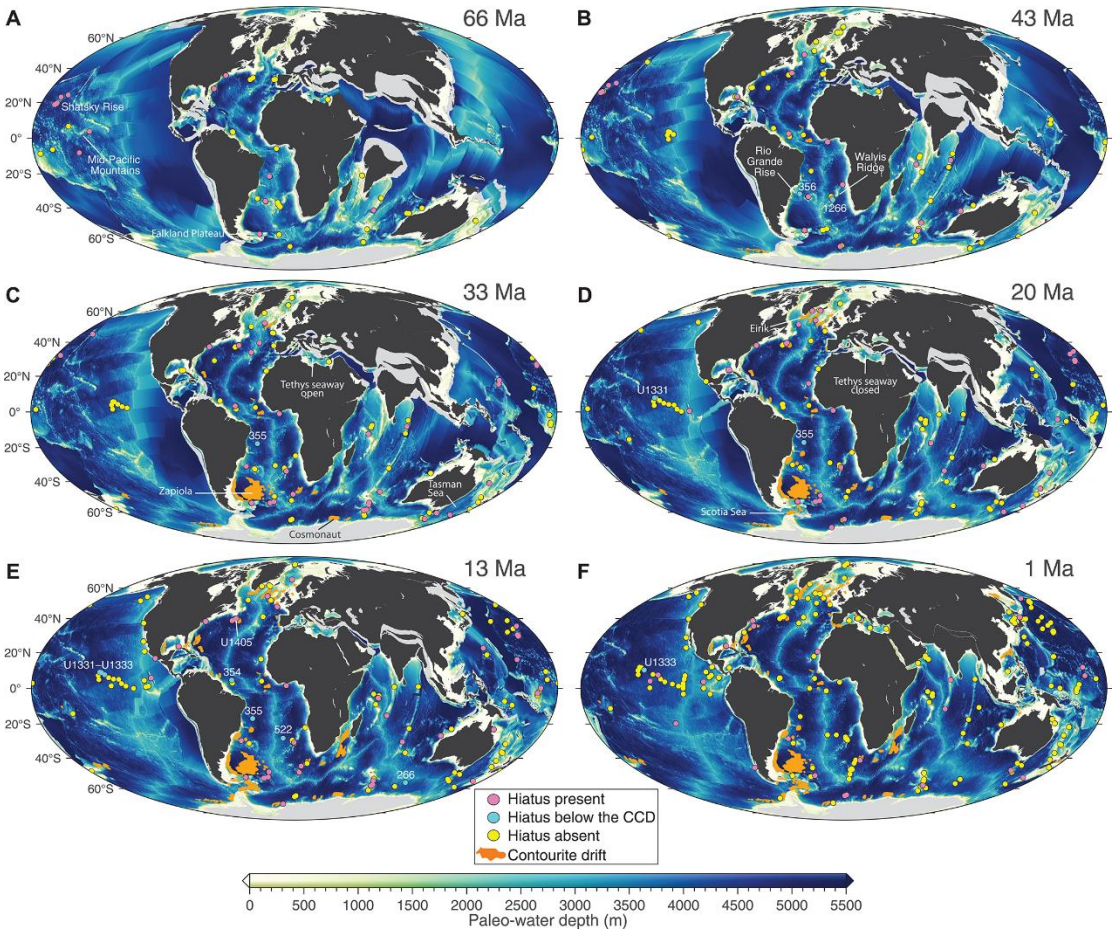

Figure 3. Distribution of backtracked sites with deep-sea hiatuses (pink dots) and their paleo–water depths for key time slices. Sites with hiatuses formed below regional carbonate compensation depth (CCD) (see Fig. 2D) are shown as cyan dots with Deep-Sea Drilling Project, Ocean Drilling Program, and Integrated Ocean Drilling Program site numbers. Sites with non-hiatuses are shown as yellow dots. Orange regions indicate contourite drifts based on estimated maximum ages of their formation from compilation of Thran et al. (2018). Paleobathymetry of preserved seafloor is reconstructed using pyBacktrack version 1.4 (Müller et al., 2018b), while paleo–water depths of now-subducted ocean floor (smooth regions) are based on Wright et al. (2020), with all grids including dynamic topography from model "M7" (Müller et al., 2018a). See Video S1 (see footnote 1) for reconstructions at 1 m.y. intervals.